



HAL
open science

Heavy-water-based moderator design for an AB-BNCT unit using a topology optimization algorithm

Sébastien Chabod, Julien Giraud, Marine Hervé, Daniel Santos, Nadine Sauzet

► **To cite this version:**

Sébastien Chabod, Julien Giraud, Marine Hervé, Daniel Santos, Nadine Sauzet. Heavy-water-based moderator design for an AB-BNCT unit using a topology optimization algorithm. *Physics in Medicine and Biology*, 2022, 67 (10), pp.105009. 10.1088/1361-6560/ac6723 . hal-03668903

HAL Id: hal-03668903

<https://hal.science/hal-03668903>

Submitted on 17 Nov 2022

HAL is a multi-disciplinary open access archive for the deposit and dissemination of scientific research documents, whether they are published or not. The documents may come from teaching and research institutions in France or abroad, or from public or private research centers.

L'archive ouverte pluridisciplinaire **HAL**, est destinée au dépôt et à la diffusion de documents scientifiques de niveau recherche, publiés ou non, émanant des établissements d'enseignement et de recherche français ou étrangers, des laboratoires publics ou privés.

Heavy-water-based moderator design for an AB-BNCT unit using a topology optimization algorithm

Sébastien Chabod, Julien Giraud, Marine Hervé, Daniel Santos, Nadine Sauzet
Univ. Grenoble Alpes, CNRS, Grenoble INP, LPSC-IN2P3, 38000 Grenoble, France
Postal address: LPSC, 53 avenue des Martyrs, 38026 Grenoble, France
Email address: sebastien.chabod@lpsc.in2p3.fr
ORCID ID: <https://orcid.org/0000-0003-2154-2012>

Abstract.

Objective. The design of neutron moderators for BNCT treatment units currently relies on parametric approaches, which yield quality results but are ultimately limited by human imagination. Efficient but non-intuitive design solutions may thus be missed out. This limitation needs to be addressed. *Approach.* To overcome this limitation, we propose to use a topology optimization algorithm coupled with a state-of-the-art Monte-Carlo transport code. This approach recently proved capable of finding complex optimal configurations of particle propagators with limited human intervention. *Main results.* In this study, we apply this algorithmic solution to optimize some heavy-water neutron moderators for a specific AB-BNCT treatment unit. The moderators thus generated are compact yet succeed in limiting the exposure of patient's healthy tissues to levels below recommended limits. They present subtle, original geometries inaccessible to standard parametric approaches or human intuition. *Significance.* This approach could be used to automatically fit the design of a BNCT moderator to the location and shape of the tumor or to the morphology of the patient to be treated, opening a path for more targeted BNCT treatment.

Key words: boron neutron capture therapy, neutron moderator, topology optimization.

1. Introduction

Context. Boron Neutron Capture Therapy (BNCT) is a radiotherapy technique that uses a field of epithermal neutrons to treat deep-seated and/or diffuse tumors [1-4]. In the early days, these fields were generated by nuclear reactor cores, limiting the use of this approach to a small number of sites, the number of which is also declining with the decommissioning of a growing number of research reactors. The development of compact accelerator-based neutron sources that can be deployed in a hospital environment is removing this limitation, leading to renewed interest in this approach, renamed Accelerator-Based BNCT (AB-BNCT). Concretely, a patient absorbs before treatment a boron-10 delivery agent, which targets preferentially cancer cells. Boron-10 captures neutrons with a high cross-section (~ 3800 barns at 0.025 eV) and splits into 2 nuclei, ^4He and ^7Li , with a probability of 94% both carrying 2.3 MeV of kinetic energy and 6% carrying 2.78 MeV. These heavy charged particles stop after a short track ($\sim 5\text{-}8\ \mu\text{m}$) through tissue, depositing most of their energies in the cancerous cells, destroying them. Some amount of boron-10, however, remains in the patient's blood and healthy tissue, leading to an unwanted exposure in the neutron field. In addition, the primary and secondary particles that propagate in the treatment unit and in the patient induce potentially damaging exposure, which should be kept to a minimum [5]. For these reasons, the BNCT neutron sources, which emit mostly epithermal to fast neutrons, must be assisted by moderators, which lower the energies of neutrons to levels less risky for healthy tissue, $\sim 0.5\text{-}10$ keV. The scientific and technological challenges that must be addressed to make AB-BNCT available, efficient and safe, therefore include (1) the development of intense compact neutron sources, (2) the development of targets that can withstand a high beam power ($\sim 30\text{-}75$ kW), necessary to reduce the treatment time to the order of one hour; (3) the synthesis of boron delivery agents allowing a higher contrast between the concentration in ^{10}B in the tumor and the healthy tissue; (4) improving knowledge on neutron and photon transport, and on the calculation of deposited doses and their biological effects; (5) high-accuracy monitoring of the doses delivered to patients; (6) the development of

compact neutron moderators capable of adjusting their energies and directions to target a tumor while best preserving healthy tissue. The present study addresses this last issue (6).

Aim of the study. The design of BNCT moderators currently relies on parametric approaches. First, a set of potential configurations is assembled, by varying the composition and dimensions of their components. The choice of these configurations is based in part on the analysis of neutron-matter interaction cross-sections, in part on human intuition and experience. For each possible configuration, a simulation of the treatment unit is then performed, using Monte-Carlo codes nowadays. Moderator configurations that offer interesting compromises between chosen therapeutic and economic objectives are thus identified, and possibly refined. These parametric studies yield interesting, multi-material design solutions, which deliver high tumor doses while keeping the doses deposited in healthy tissues under control [6-8]. However, being constrained by human creativity, they can only explore a small fraction of the solution space, and may thus miss out on more efficient but unintuitive designs. For intermediate to deep-seated tumors e.g., parametric based designs cannot yet prevent the deposition of large doses in upstream tissues, in particular in the scalp during the treatment of glioblastoma. Therefore, an approach that would allow the space of possible configurations to be explored with little to zero human bias could provide the BNCT community with innovative design solutions. For this purpose, we will leave in this study the determination of the design of a heavy-water neutron moderator in the hands of a topology optimization (TopOpt) algorithm, the principle of which will be described in section 3.1. Examples of successful applications of this TopOpt approach will be presented in sections 3.2 and 3.3.

Additional information. In Appendix are gathered sensitivity studies required to evaluate the robustness of the TopOpt computations performed in this study. We discuss there the global character of the optimal configurations of heavy-water moderators generated by the algorithm, and evaluate among other questions of interest the sensitivity of the quality of treatment to the uncertainties on transport data or to the morphological diversity of the patients.

Computation means. The simulations carried out for this study were run on servers with 24 modern CPUs (+24 virtual), dating from the end of the 2010s, at the rate of one simulation per server. The computation times mentioned in the rest of this study correspond without exception to the durations of the computations launched on these machines.

2. Modeling of the treatment unit

In this section are presented the models, data and codes used for computing the structure of a BNCT neutron moderator and its performances, for a specific configuration described below.

2.1. Neutron source

For this study, we consider one of the main neutron sources envisaged for an AB-BNCT treatment unit, which makes use of the ${}^9\text{Be}(d(1.45\text{ MeV}), n)$ reaction [9]. This reaction produces neutrons with good efficiency, 3.3×10^{11} neutrons/mC, with a not too hard energy spectrum, and its manufacture and operation at high power are considered less challenging than ${}^7\text{Li}(p,n)$ sources [7]. The deuteron beam, here parallel to the Y axis, is assumed to be uniformly distributed over the surface of the ${}^9\text{Be}$ target, a 10 cm^2 disc visible fig. 1 at $x = -6.7\text{ cm}$. Such a surface is considered necessary to dissipate the high power deposited by the beam, expected to

be ~ 40 kW. The ^9Be deposit is assumed to be homogeneous. Therefore, in our simulations, the neutron emission coordinates are sampled uniformly across the surface of the target disk.

The energy and angle distribution of the generated neutrons for a $9\ \mu\text{m}$ thick thin target was measured by Capoulat et al. and is given in the fig. 4 of Ref. [9]. This distribution, which shows a maximum below ~ 0.4 MeV whatever the angle and a tail of fast neutrons up to ~ 6 MeV, is rigorously implemented in the transport code used for this study, MCNP 6, by using the functionalities of its SDEF card [10]. The target casing model, simplified for study purposes, is an aluminum and graphite structure, in yellow fig. 1. Between the casing and the moderator is inserted a layer of lead, in blue fig. 1, to reduce the fluence of primary gamma rays.

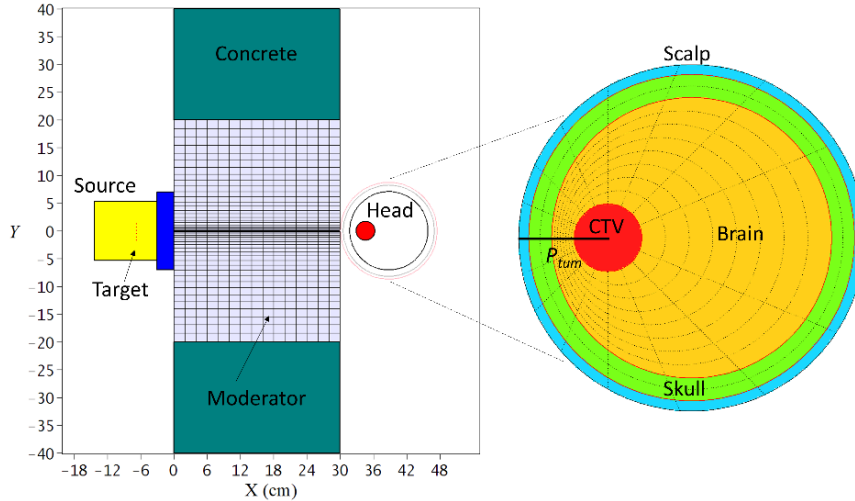


Figure 1. (Left) simplified models of the neutron source (yellow), the biological protection (blue), the concrete wall (green), the moderator and its voxelization (gray), the patient's head and the CTV (red) ; (right) simplified model of the patient's head, with its voxelization: CTV (red), normal brain (orange), skull (green), scalp (blue).

2.2. General characteristics of the neutron moderator

A $^9\text{Be}(d(1.45\ \text{MeV}), n)$ source generates neutrons of ~ 2 MeV in average, up to ~ 6 MeV, which must be slowed down to the desired energies for a BNCT treatment, ~ 0.5 - 10 keV, in order to reduce the neutron dose in the healthy tissues. This moderation must be carried out in a device with a low footprint, compatible with use in a hospital environment. Such a moderator must thus be manufactured mainly using materials having light nuclei or large inelastic scattering cross-sections. For this case study, we propose to optimize the structure of a moderator made of heavy water, 99% atomic pure. Heavy water is an interesting material for several reasons: (i) it has excellent neutron moderating power, ^2H having a low nucleus mass, close to that of the neutron; (ii) ^2H has a low neutron capture cross-section, which increases the output neutron fluence and reduces the production of dosing capture gamma rays; (iii) being liquid, D_2O is well suited to the manufacture of topologically optimized moderators, which can be fitted to the tumor configuration or to the morphology of the patient to be treated. Heavy water has already been used in a beam shaping assembly even if not as main or exclusive component [11]. Its use was recently studied by Hervé et al., who showed during a parametric study that a hemispherical moderator made of heavy water presented the best tumor dose over brain dose ratios for most of the parameters they explored (composition and radius of the moderator, depth of the tumor) [8].

The heavy water moderator, with a maximum radius of 20 cm and a length of ~ 30 cm (variable), is inserted into a heavy concrete wall, in green fig. 1, which serves as biological protection. In order to limit the computation time, this moderator has an axis of symmetry, coinciding with the axis of the beam. Unless otherwise stated, the moderator will be segmented into $N = 375$ voxels $\Theta_j = 1 \dots N$ (25 steps in length, 15 in radius). These voxels, drawn in fig. 1, are cylindrical crowns with axis that of the beam, each containing a density ρ_j of heavy water varying between 0 and 1.11 g/cm^3 , the natural density of heavy water. The objective of the study is to find the densities ρ_j that optimize the BNCT treatment quality, using a topology optimization algorithm.

2.3. Patient's modeling

For this study, we will consider the case of the treatment of glioblastoma. We will only model the patient's head, simplifying its composition. Only the brain, skull and scalp are modeled, using spheres with radii 7.05 cm, 8.21 cm and 8.71 cm, visible in fig. 1. These average radii, consistent with anatomical data for a standard adult human [12, 13], give volumes of brain, skull and scalp equal to those of a Snyder's model [14].

The Clinical Target Volume (CTV) containing the tumor is modeled by a sphere of volume 20 cm^3 , represented in red fig. 1. This sphere is positioned at a depth P_{tum} , defined as being the smallest distance between the center of the CTV and the surface of the patient's head, cf. fig. 1. Its center is on the axis of the beam. The center of the patient's head is also on the axis of the beam, at a distance chosen so that the minimum distance between the surface of the head and the right side of the moderator is equal to 1 mm, cf. fig. 1 (quasi contact to minimize neutron losses).

The patient's head is subdivided into $M = 89$ voxels $\Delta_i = 0 \dots 88$: 1 voxel Δ_0 for the tumor, 88 others for normal tissues (64 for the brain, 16 for the skull, 8 for the scalp). These 88 voxels are delimited by: (i) cones whose vertices are the center of the CTV and whose opening angles vary between 0° and 180° ; (ii) and ellipsoids of revolution, whose axes of symmetry coincide with that of the beam, and whose ends are chosen to regularly pave the patient's head. This paving is presented in fig. 1 (right).

The choice of this head model is motivated by several constraints:

- (i) *the computation time*: the time required for the optimization algorithm to converge increases with the number M of voxels used to pave the head, in $\sim 4M$ for M small. For $M \gg 1$, this time is expected to increase exponentially with M . Thus, for 89 voxels Δ_i for the head and 375 voxels Θ_j for the moderator, it takes 2 months of computation on a 24 CPU server to determine the optimal structure of the moderator. Without axial symmetry, it would be necessary to add a discretization in angle φ around the axis of symmetry, by cutting the structure using planes containing the axis of the beam. By taking for example 10 angles φ , the number M of voxels would increase to 881, and the computation time to ~ 20 months on a 24 CPU server;
- (ii) *uncertainty on the volume of tissue concerned by a peak dose*: axial symmetry eliminates the uncertainty on the volume of tissue affected by a peak dose, most often not provided in the literature. Indeed, by cutting the model of the patient's head using planes containing the axis of symmetry, again, we can subdivide each voxel Δ_i into an arbitrarily large number of sub-voxels, of arbitrarily small volumes but nevertheless all exposed to the same dose;
- (iii) *sensitivity to morphological variability*: analytical models, e.g. of the Snyder type, are quite rigid, and their representativeness for all patients may raise debate. In order to study the impact of the morphological variability of patients on the quality of their treatments, the head model considered in this study can be of interest. This sensitivity study is presented in Appendix A.3.

2.4. Biological dose

To evaluate the biological doses deposited in each voxel of the head, we will use the ICRU 46 compositions and densities of the tissues, recalled in Table 1 of Ref. [14]. The composition of the tumor will differ from that of the brain only in its higher concentration of ^{10}B . The ^{10}B delivery agent considered is BPA, the corresponding ^{10}B concentrations C_B are given in Table 1 for each tissue (factor 1 brain/blood, 3.5 tumor/blood, 1.5 scalp/blood) [7].

In this study, we will use a standard definition of the total biological dose, $D = w_n D_n + w_B D_B + w_\gamma D_\gamma$, where $D_{n,B,\gamma}$ are the neutron, boron and gamma doses, and $w_{n,B,\gamma}$ the corresponding biological weighting factors, given in Table 1 for each tissue [8]. To evaluate each dose component $D_{n,B,\gamma}$, we will use kerma factors for each tissue. The supplementary material of Ref. [14] contains files which allow to reconstruct the neutron kerma, $K_n(E)$, using the elementary neutron kerma given Ref. [15, 16], for each tissue. These kerma factors notably take into account the contributions of the $^{14}\text{N}(n,p)$ or $^{\text{nat}}\text{Cl}(n,p)$ reactions. The K_n curves obtained are presented in fig. 2 (left). The gamma dose is calculated under charged-particle equilibrium [17]. The K_γ photon kerma are reconstituted for each tissue using Ref. [18] and log-log fits for the missing energy intervals. We checked that this approach exactly returns the photon kerma for the brain provided in Ref. [19]. The photon kerma obtained for each tissue are shown fig. 2 (right). Finally, the K_B boron kerma comes from [14], and is given in fig. 2 (left) per ppm of ^{10}B in tissue. The equation for the total biological dose D_i in each voxel Δ_i of the patient's head is thus written:

$$D_i = w_{n,i} D_{n,i} + w_{B,i} D_{B,i} + w_{\gamma,i} D_{\gamma,i}$$

$$= \int_E \left[\left(w_{n,i} K_{n,i}(E) + w_{B,i} K_{B,i}(E) \right) \phi_{n,i}(E) + w_{\gamma,i} K_{\gamma,i}(E) \phi_{\gamma,i}(E) \right] dE \quad (1)$$

where $\phi_{n,i}(E)$ and $\phi_{\gamma,i}(E)$ are the neutron and photon fluences per unit of energy in the voxel Δ_i .

Tissue	RBE w_n	CBE w_B	w_γ	C_B ($\mu\text{g/g}$)
tumor	3.2	3.8	1	52.5
brain	3.2	1.3	1	15.0
skull	3.2	1.3	1	15.0
scalp	3.2	2.5	1	22.5

Table 1. Biological weighting factors $w_{n,B,\gamma}$ and ^{10}B concentrations C_B (in $\mu\text{g/g}$) in head tissues.

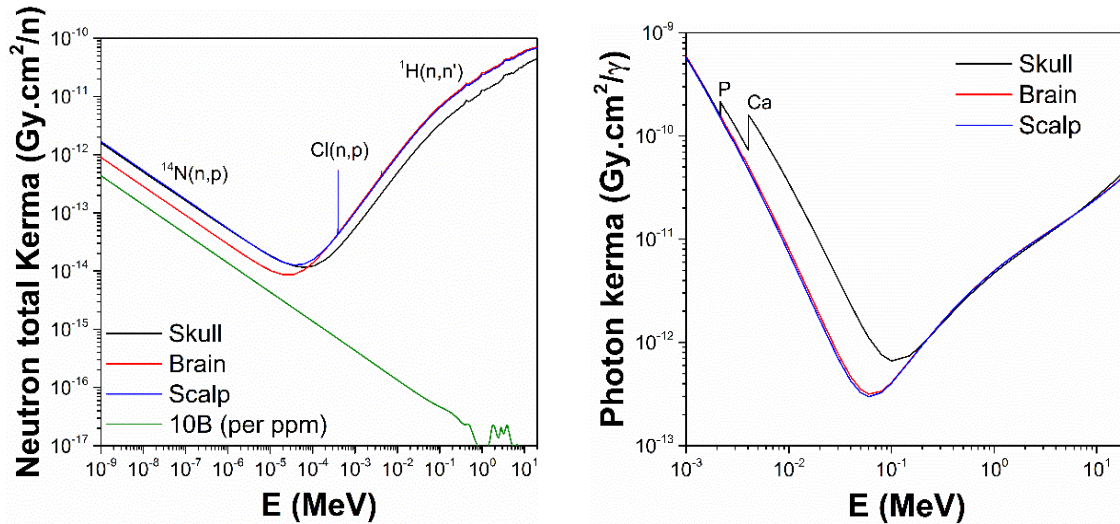


Figure 2. (Left) neutron kerma, $K_n(E)$, in $\text{Gy}\cdot\text{cm}^2/\text{neutron}(n)$ in the brain, the skull and the scalp; boron kerma, in $\text{Gy}\cdot\text{cm}^2/\text{neutron}(n)$, per ppm of ^{10}B in a tissue; (right) photon kerma, $K_\gamma(E)$, in $\text{Gy}\cdot\text{cm}^2/\text{gamma}(\gamma)$, in the brain, the skull and the scalp.

2.5. Peak doses

The values of the peak doses not to be exceeded locally, available in the literature for the brain, skull or scalp, vary significantly from one study to another, and rarely mention the volume of tissue concerned. They are summarized in Table 2. The value of the peak dose for the brain, $L(\text{brain}) = 14.1 \pm 1.8 \text{ Gy-Eq}$, used by Hervé et al. comes from a study by Coderre et al., which showed that exposure of 14.1 Gy-Eq in 1 cm^3 of brain induces in 50% of treated patients a somnolence syndrome [5]. This proportion is reduced to 5% for $L(\text{brain}) = 11 \text{ Gy-Eq}$ (1 cm^3 of brain) [5], a more acceptable proportion if BNCT were to develop, which is the value used by Capoulat et al. [7]. The values of the peak doses for the scalp, $L(\text{scalp}) = 16.7$ and 24 Gy-Eq , respectively used by Capoulat et al. and Torres-Sánchez et al. are consistent with the findings of a study by Menéndez et al., which shows that doses to the skin between 16.5 and 24 Gy-Eq have manageable toxicities [21]. The study by Menéndez et al. however concerns a small number of patients, whose area treated with BNCT was not the scalp but various leg skins. The transposition of the results of [21] to the determination of $L(\text{scalp})$ is therefore not immediate.

References	Peak dose L (Gy-Eq)			Comment
	brain	skull	scalp	
Torres-Sánchez et al. [6]	12.5	∞	24.0	No indication of the volume of tissue concerned
Capoulat et al. [7]	11.0	∞	16.7	No indication of the volume of tissue concerned
Hervé et al. [8]	14.1 ± 1.8	∞	∞	Peak dose valid for 1 cm^3 of tissue
Rubin [20]	15-25	> 30	15-20	Single photon dose, value for scalp is for skin
This study	11.0	30.0	16.7	Choice of the most conservative values

Table 2. Values of the peak doses not to be exceeded locally for the brain, skull and scalp, in the literature [6, 7, 8, 20]. The peak doses used in this study are given in the last line.

In conclusion, as a precaution, we will use in this study the most conservative L values proposed in the literature, indicated last line of Table 2. These conservative values pose an interesting challenge to the design of the moderator, which should ensure a high contrast between the tumor dose and the doses deposited in healthy tissues.

2.6. Transport code and nuclear data

The simulations carried out for this case study were performed with the transport code MCNP 6 [10], simultaneously propagating neutrons and photons. The neutron and photon transport data used come from the ENDF/B-VII.0 database (/B-VI.6 for ^1H and ^{138}Ba). All cross-sections, including $S(\alpha,\beta)$ data, are taken at room temperature. An analysis of the impact of the choice of the transport data is carried out in Appendix A.2. With the exception of calculations performed with $N = 150$ voxels, all MCNP simulations performed in this study were run using 5×10^9 source neutrons.

3. Topology optimization of the moderator

In this section, we will let a topology optimization algorithm determine the structure of an AB-BNCT heavy water neutron moderator, with a level of human intervention as low as possible. Still, choices will have to be made, which like any human choice are debatable, and amendable if necessary. We will choose to optimize the structure of a D_2O moderator, favoring, over all other considerations, the cleanliness of the treatment, i.e. the ability of the AB-BNCT unit: (i) to generate a high dose in the tumor; (ii) while ensuring that the doses deposited in the patient's head do not exceed the local peak doses, or exceeds them as little as possible if this goal proves untenable. This choice, which gives priority to the therapeutic objective over the economic objective, will lead to moderator configurations that will not necessarily maximize the dose rate deposited in the tumor, and therefore will not minimize the treatment time. This choice is present in the watermark in many studies of moderator design, cf. e.g. [6-8]. In part because treatment time is function of the maximum beam power, which itself depends on manufacturing processes and technological innovations not all off the shelf. Partly also because there is no rigid guideline on this treatment time. Some recommend it to be less than 60 min, but what about the possibility of multi-fractionating the treatment for example. In the absence of certainty on this subject, the choice made in section 3 seems reasonable. It is however important to note that an optimization of the moderator design with a different objective, e.g. an objective of minimizing the treatment time, can be carried out using the same methodology than that presented in section 3.1, by simply replacing the F_{PEN} function in Eq. (2) by the treatment time.

3.1. Formalization and resolution of the optimization problem

We want to determine the optimal composition of a D_2O moderator, i.e. to find the optimal densities ρ_j of heavy water contained in each voxel Θ_j , which simultaneously allow a D_{obj} dose to be deposited in the tumor while minimizing the exposure of healthy tissues. To achieve these goals, we must ensure that each dose D_i , given Eq. (1), deposited in each voxel Δ_i of the patient's head does not exceed the corresponding peak dose L_i . As a reminder, cf. Table 2, $L_i = 11 \text{ Gy-Eq} \forall \Delta_i \in \text{brain}$, $30 \text{ Gy-Eq} \forall \Delta_i \in \text{skull}$ and $16.7 \text{ Gy-Eq} \forall \Delta_i \in \text{scalp}$.

This complex problem can be formalized as follows:

$$\min_{\underline{\rho}} F_{PEN}(\underline{\rho}) = \sum_{i=1}^M \alpha_i \left(D_i(\underline{\rho}) / L_i \right)^n, \quad \alpha_i = \frac{V_i}{V_{head}}$$

$$D_i(\underline{\rho}) = \frac{1}{V_i} \int_{E=0}^{+\infty} \int_{\underline{\Omega} \in 4\pi} \int_{\underline{r} \in \Delta_i} \left[\begin{array}{l} w_B(\underline{r}) K_B(\underline{r}, E) \\ + w_n(\underline{r}) K_n(\underline{r}, E) \\ + w_\gamma(\underline{r}) K_\gamma(\underline{r}, E) \end{array} \right] \varphi_n(\underline{r}, E, \underline{\Omega}, \underline{\rho}) d\underline{r} dE d\underline{\Omega} \quad (2)$$

s.t. $B_n(\underline{\rho}) \varphi_n = Q_n$ (C₁), $B_\gamma(\underline{\rho}) \varphi_\gamma = Q_\gamma(\varphi_n)$ (C₂)
 $D_0(\underline{\rho}) = D_{obj}$ (C₃) $\rho_j \leq \rho_{max} \forall j$ (C₄)

or, put in a form which calls upon its Lagrangian L and a vector of multipliers $\underline{\lambda}$:

$$L = F_{PEN} - \underline{\lambda} \cdot \underline{C}$$

$$\frac{\partial L}{\partial \underline{\rho}} = \underline{0}, \quad \frac{\partial L}{\partial \underline{\lambda}} = \underline{0} \quad (3)$$

Eq. (2)-(3) consists in finding the D₂O densities, $\underline{\rho} = (\rho_1, \dots, \rho_N)$, of the moderator voxels that minimize a penalization function F_{PEN} , while respecting 4 constraints \underline{C} , described below:

Penalization function: function F_{PEN} quantifies the cleanliness of the treatment: the lower its value, the more the treatment respects the peak doses in normal tissues. Concretely, for each voxel $\Delta_i > 0$ of the patient's head, F_{PEN} is incremented by a quantity $(D_i/L_i)^n$ weighted by the volume V_i of the voxel, V_{head} being the volume of the head. By taking a number $n \gg 1$, F_{PEN} is therefore incremented by a small quantity if $D_i < L_i$, since $x^n \rightarrow 0$ if $x < 1$, $n \rightarrow +\infty$, and on the contrary by a quantity high if $D_i > L_i$, since $x^n \rightarrow +\infty$ if $x > 1$, $n \rightarrow +\infty$. We will take $n = 30$ in this study. An analysis of the impact of this choice is carried out in Appendix A.1.

Constraint C₁: the neutron transport must obey the linear Boltzmann equation, $B_n(\underline{\rho}) \varphi_n = Q_n$, where B_n is the Boltzmann operator, a function of the physicochemical characteristics of the materials crossed, therefore of the densities $\underline{\rho}$. Function $\varphi_n(\underline{r}, E, \underline{\Omega}, \underline{\rho})$ is the angular fluence of neutrons at position $\underline{r} = (x, y, z)$, of energies E and directions $\underline{\Omega}$. The Q_n term is the distribution in positions, energies and directions of the neutrons generated by the source, as a reminder ${}^9\text{Be}(d(1.45 \text{ MeV}), n)$ for this study.

Constraint C₂: the photon transport must also obey a Boltzmann equation, with a source term Q_γ depending on the neutron fluence (production of gammas by neutron interactions).

Constraint C₃: the dose D_0 deposited in the tumor must be equal to D_{obj} , equal to 30 Gy-Eq for a single-fraction glioblastoma treatment, cf. pp 201 of [1].

Constraint C₄: the D₂O densities $\rho_{j=1\dots N}$ can vary between 0 and $\rho_{max} = 1.11 \text{ g/cm}^3$, the natural D₂O density.

Eq. (2)-(3) is a constrained optimization problem of which we can see the extreme complexity. The F_{PEN} function is a non-linear functional of the angular fluences of neutrons and photons, themselves non-linear, highly complex functionals of the densities $\underline{\rho}$ of the moderator. The space of solutions to be explored is also gigantic: for 375 voxels, each containing a density

varying between 0 and ρ_{max} , say by small step $\delta\rho = \rho_{max}/50$, the number of possible moderator configurations is worth $50^{375} = 1.3 \times 10^{637}$, that is to say a numerical infinity. Despite this extreme complexity, it is now possible to solve Eq. (2)-(3) in a humanly compatible time using the topology optimization (TopOpt) algorithm presented in Ref. [22, 23].

This algorithm can organize a material to optimize the transport of particles passing through it, in the framework of the linear Boltzmann equation, according to design objectives / constraints. It builds on the sensitivity calculation module of MCNP 6, which makes it possible, among other things, to compute the derivatives of a particle flux with respect to cell densities, therefore to compute the derivatives appearing in Eq. (3) [10]. It has been previously used to compute the structure of several nuclear devices, including a neutron shield, a gamma-ray collimator or a neutron spectrum shaper, with results outperforming parametric approaches [22, 23].

Concretely, this algorithm solves Eq. (2)-(3) numerically using an iterative procedure. Starting at iteration 0 from a uniform density in all moderator voxels, $\rho_j = \rho_0 \forall j$, it gradually modifies at each iteration, small step $\pm\delta\rho$ by small step, the densities ρ_j in the voxels Θ_j until reaching the solution of Eq. (2)-(3). The doses $D_{n,i}$, $D_{\gamma,i}$ and $D_{B,i}$ which make up each dose D_i , cf. Eq. (1), can be calculated with MCNP 6 using its DE and DF cards [10]. The calculation of the derivatives $\partial F_{PEN}/\partial\rho_j$ that appear in Eq. (3) involves $M \times N$ derivatives $\partial D_i/\partial\rho_j$, which can all be computed in a single MCNP 6 simulation using its PERT card [10] and the procedure described in section 1 of Ref. [22]. In this study, we took $\delta\rho = \rho_{max}/50$ and $\rho_0 = 0.2 \text{ g/cm}^3$.

3.2. Example of application of the TopOpt approach

To illustrate the operation of this TopOpt algorithm, we propose to determine in this section the optimal composition of a D₂O moderator for a 20 cm³ CTV at a depth $P_{tum} = 4.5 \text{ cm}$, cf. section 2. We will take for this calculation $N = 375$ voxels for the moderator and $M = 89$ voxels for the patient's head. The thickness H of the moderator and the heavy concrete wall is set at 30 cm, cf. fig. 1. For this configuration, the algorithm converges in 95 iterations, which required 2 months of calculation.

3.2.1. Configuration and performances of the moderator after convergence

Fig. 3 (left), we present in the XY plane some moderator configurations obtained before and after convergence for iteration numbers NUMITER ranging from 0 (starting configuration, $\rho_j = 0.2 \text{ g/cm}^3 \forall j$) to 95 (convergence). The 3D structure of the moderator is generated by rotating these graphs around the $Y = 0$ axis of symmetry. The gray scales in fig. 3 (left) give the densities ρ_j in D₂O, in g/cm^3 , in the voxels Θ_j of the moderator. Fig. 3 (center), we present the maps of the total doses D_i associated with these moderators, deposited in each voxel Δ_i of the patient's head. The color scales in fig. 3 (center) give the values of the D_i doses in Gy-Eq. Finally, fig. 3 (right), we present the values of the dose excesses, $E_i = (D_i - L_i)/L_i$, in each voxel of the head, where L_i is as a reminder the value of the peak dose in the voxel Δ_i . The color scale in fig. 3 (right) gives the values of E_i in percent. For $E_i < 0$, the objective of the moderator optimization, the voxel is colored white. So, in summary, the more white and blue in these maps, the cleaner the treatment. These figures show how the TopOpt algorithm improves iteration after iteration the structure of the moderator to improve the treatment cleanliness. At convergence, the total dose rate deposited in the tumor, denoted D_{tum} , is equal to 1.05 fGy-Eq/source neutron (s.n.). The efficiency of a ⁹Be(d(1.45 MeV), n) source being 3.3×10^{11} neutrons/mC [4], for a beam intensity of 30 mA [4], the treatment time necessary to deposit 30 Gy-Eq in the tumor will be 48 min. This time could be further reduced by adding to the simplified model of the unit

treatment shown fig. 3 a reflector around the source at $x < 0$ cm. Indeed, a fraction of the source neutrons are emitted at angles greater than 90° , and are therefore artificially lost.

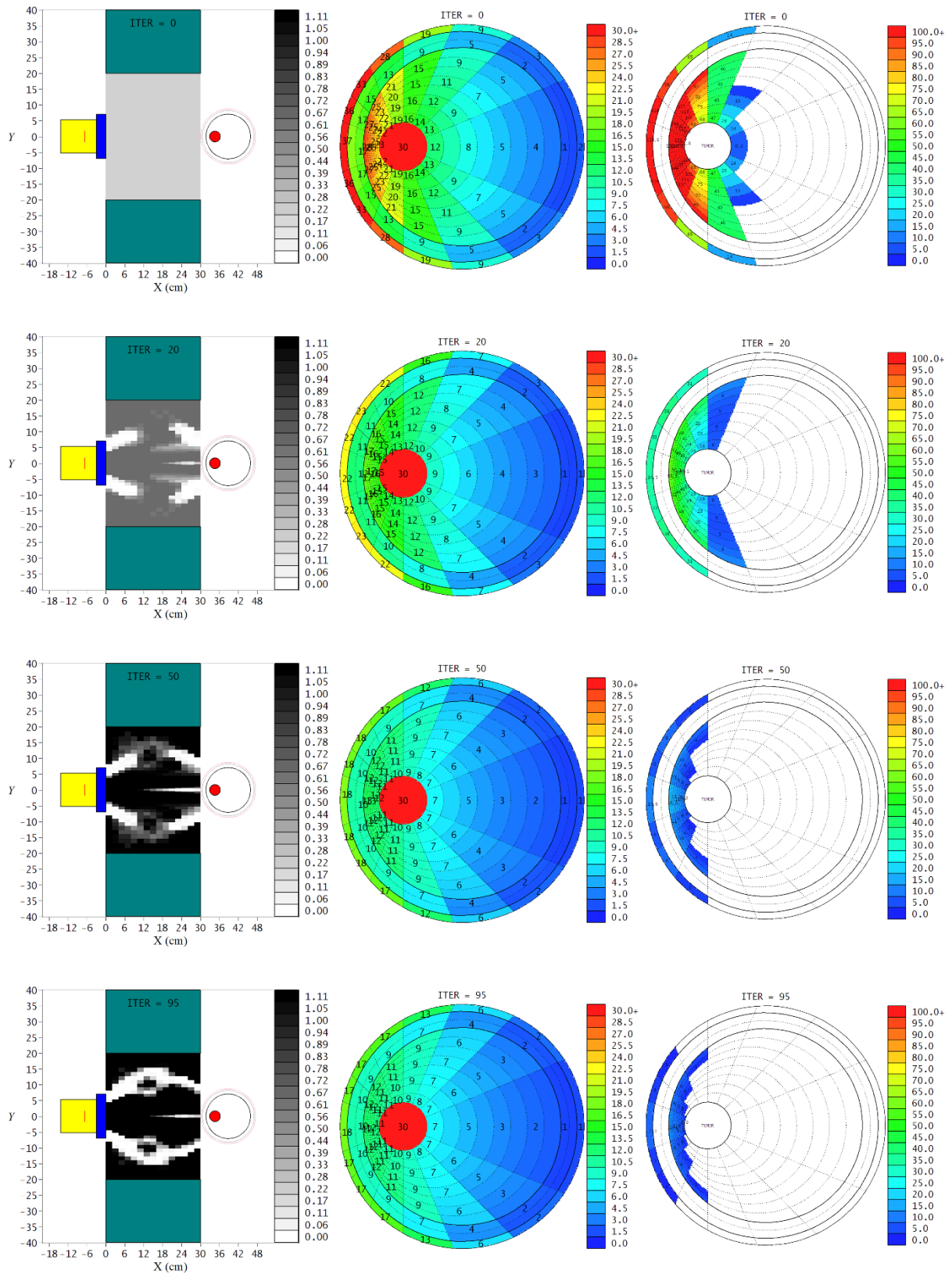


Figure 3. (Left) D₂O moderator configurations obtained for $N = 375$ voxels, $P_{tum} = 4.5$ cm, $H = 30$ cm and NUMITER = 0, 20, 50 and 95; (center) corresponding maps of the total doses, D_i , in Gy-Eq deposited in the patient's head; (right) corresponding maps of the dose excesses, E_i , in percent.

3.2.2. Optimal dose-volume histograms in normal brain and scalp

Fig. 9 (curve in green for $H = 30$ cm), we plot for the optimal configuration of the moderator obtained at NUMITER = 95 (cf. fig. 3 or 4) the dose-volume histograms in normal brain (left) and scalp (right), indicating the peak brain and scalp doses used by Capoulat et al. and Torres-Sánchez et al. [6, 7] described in section 2. For a dose to the tumor of 30 Gy-Eq and a CTV of intermediate depth, $P_{tum} = 4.5$ cm, we find that the doses deposited in normal tissues remain mostly within the imposed limits. They exceed the peak values, 11 Gy-Eq (brain) and 16.7 Gy-Eq (scalp), only in a small volume of the brain (5.4%) and scalp (11.8%), and this by little in both cases. They nowhere exceed the peak values used by Torres-Sánchez et al., 12.5 Gy-Eq (brain) and 24 Gy-Eq (scalp), with a comfortable margin for the scalp. As for the skull, the maximum deposited dose is 9.9 Gy-Eq, well below its peak value, 30 Gy-Eq. In the end, the doses deposited exceed the peak doses of Capoulat et al. [7] only in 4.8% of the head volume.

3.2.3. Details of the moderator structure

To achieve these conclusive results with a compact moderation volume, 0.04 m^3 (20 cm radius, 30 cm in length) despite the high energy, ~ 2 MeV in average and up to ~ 6 MeV, of the ${}^9\text{Be}(d,n)$ source neutrons, the TopOpt algorithm generates a subtle device, visible fig. 3 iteration 95 or fig. 4 in more detail, composed of: (i) a neutron “tunnel”, which drives the neutrons towards the tumor while slowing them down. This tunnel contains a heavy water ring, which scatters the neutron trajectories. At its exit, it recreates in an original way the equivalent of a multi-field treatment, which consists in simultaneously exposing a patient to several moderated neutron beams with different orientations [6]; (ii) a central needle, which acts as a small tunnel of moderated neutrons, and adds another directional exposure; (iii) and a main moderation body and a reflector. The details of this sophisticated structure are inaccessible to a parametric study, let alone to human intuition, thus illustrating the potential of the TopOpt approach.

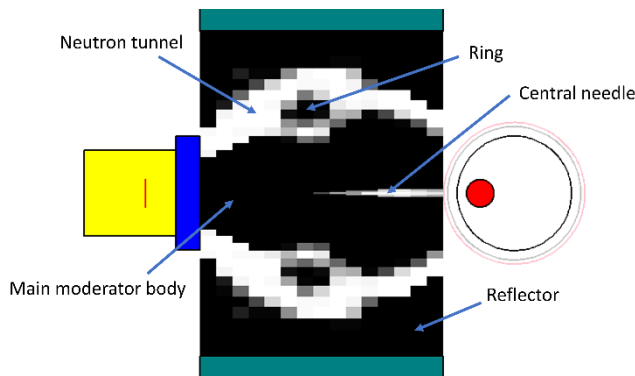


Figure 4. Details of the TopOpt moderator calculated for $N = 375$, $P_{tum} = 4.5$ cm and $H = 30$ cm.

3.2.4. Neutron, boron and gamma contributions to the deposited doses

For the moderator obtained fig. 4, we give fig. 5 the relative contributions, in the total dose D_i deposited in each voxel Δ_i of the patient's head, see section 2.4, of: (i) the boron dose, $w_{B,i}D_{B,i}/D_i$, (ii) the ${}^{14}\text{N}(n,p)$ dose, $w_{n,i}D_{14N,i}/D_i$; (iii) the neutron dose, without the ${}^{14}\text{N}(n,p)$ contribution, $w_{n,i}(D_{n,i} - D_{14N,i})/D_i$; (iv) the gamma dose, $w_{\gamma,i}D_{\gamma,i}/D_i$. The color scales in fig. 5 give these relative contributions in percent. As the ${}^{14}\text{N}(n,p)$ reactions induce $\sim 100\%$ of the total neutron dose below 10 keV, the ${}^{14}\text{N}(n,p)$ dose matches well with the thermal neutron dose, see. Ref. [14].

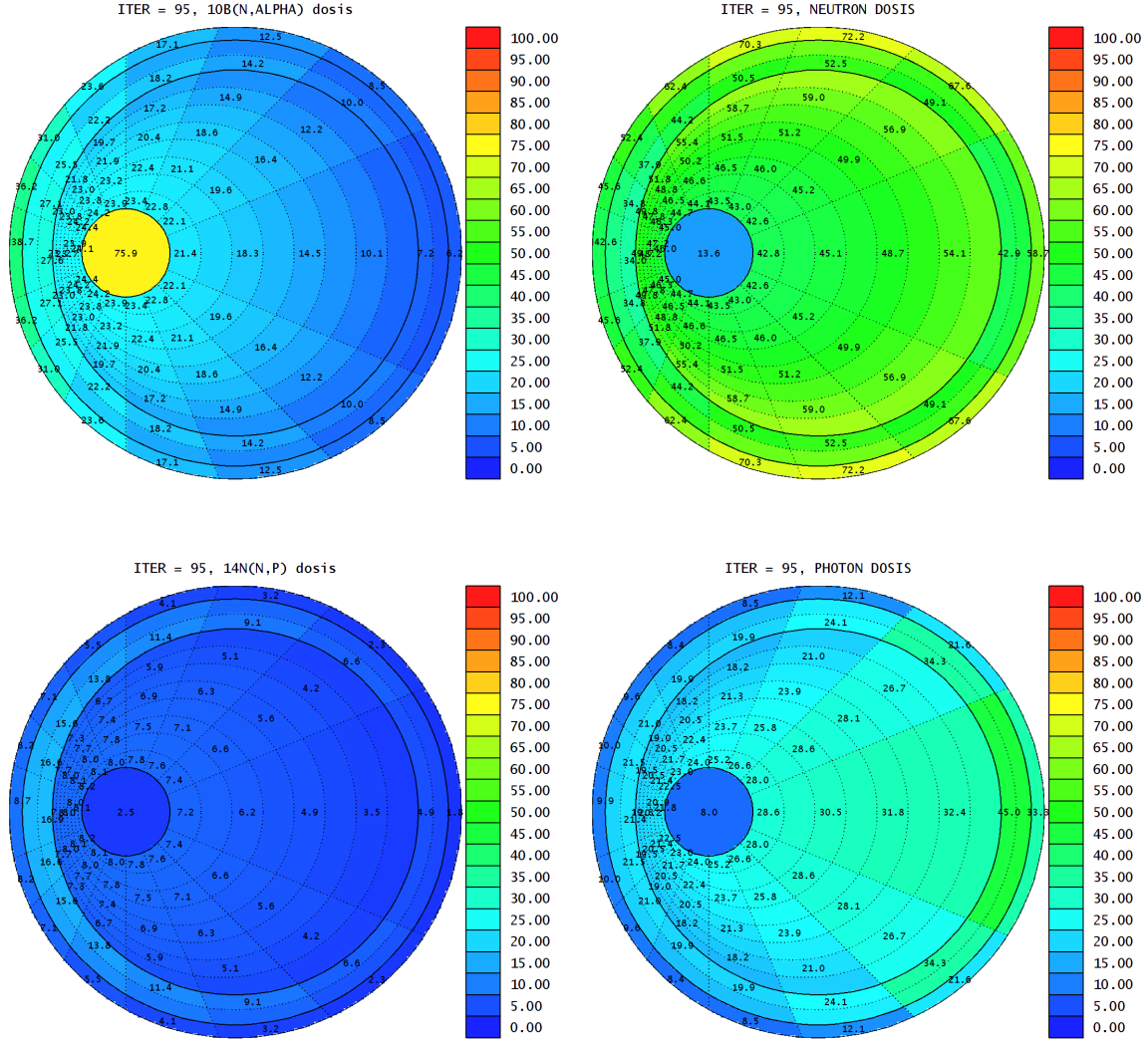


Figure 5. Relative contributions, in %, of the boron dose, the $^{14}\text{N}(n,p)$ dose, the neutron dose (w/o $^{14}\text{N}(n,p)$) and the gamma dose to the total doses D_i deposited in each voxel Δ_i of the patient's head, for the TopOpt moderator shown fig. 4, obtained for $N = 375$ voxels, $P_{tum} = 4.5$ cm and $H = 30$ cm.

We also plot in fig. 6 the evolutions of the boron dose, the $^{14}\text{N}(n,p)$ dose (thermal neutron dose), the neutron dose without $^{14}\text{N}(n,p)$ and the gamma dose, delivered in healthy (left) and tumor (right) brain tissues, as a function of the depth P in brain along the beam axis. These doses are calculated using the patient's head model described in section 2.3, without the tumor. The doses are computed inside spheres with radius of 2 mm, containing either healthy or tumor brain tissues, whose centers are positioned every 5 mm along the beam axis, inside the brain, taking as depth $P = 0$ cm the point (closest to the moderator) where the beam axis intersects with the surface of the brain. This origin, $P = 0$ cm, is therefore located at a depth of 1.66 cm from the surface of the patient's head, see section 2.3.

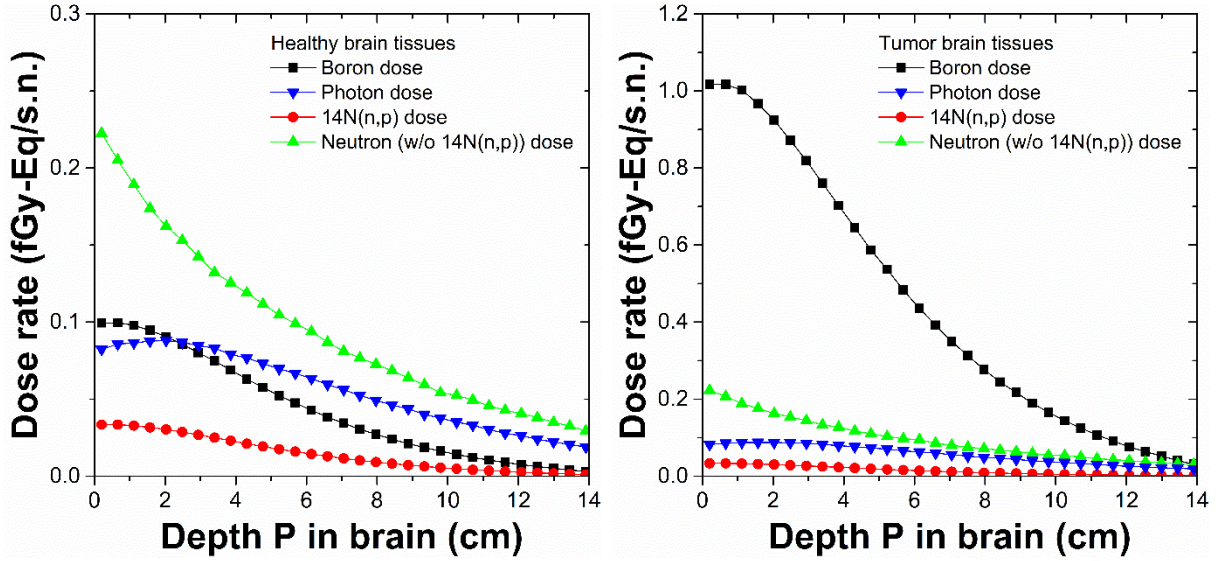


Figure 6. Evolutions of the boron, $^{14}\text{N}(n,p)$, neutron (w/o $^{14}\text{N}(n,p)$) and gamma doses, expressed in fGy/s.n., delivered in healthy (left) and tumor (right) brain tissues positioned at a depth P in brain along the beam axis. The origin, $P = 0$ cm, is on the brain surface, therefore 1.66 cm deep from the surface of the patient's head.

We observe fig. 5-6 that: (i) the boron dose represents 76% of the total dose deposited in the tumor. In healthy tissues, however, it is only really important in areas of the scalp on the beam axis, where it matches the neutron dose contribution; (ii) the negligible nature of the $^{14}\text{N}(n,p)$ dose, except in the regions of the skull facing the moderator; (iii) the dominant character of the epithermal and fast neutron dose, which accounts for $\sim 50\%$ of the total dose in all voxels except tumor, and which logically dominates in the areas of the scalp close to the exit of the neutron tunnel. The cleanness of the treatment thus strongly depends on the way in which the moderator slows down and focuses the neutrons on the head; (iv) the low relative contribution of gamma rays in the areas of the brain facing the moderator, which becomes important in its rear areas. This observation confirms the necessity to propagate neutrons and photons simultaneously in the simulations.

3.2.5. Energy spectra of neutrons at the exit of the moderator

Fig. 7, we plot some energy spectra of neutrons generated at the exit of the moderator, at 4 positions shown fig. 7 (left). We note that these spectra all contain: (i) a thermal component. It has a low impact on tissues, as shown in fig. 5, where we observe that the $^{14}\text{N}(n,p)$ contribution to the total deposited dose is low. It could nevertheless be cut by adding e.g. a thin coating of a material enriched in boron at the moderator surface; (ii) a slowing-down spectrum, from 0.2 eV up to 10-100 keV; (iii) a fast neutron component, around 1-6 MeV. The neutron tunnel (position 3) brings an additional epithermal contribution up to 200 keV. The spectrum emitted by the reflector (position 4) is a little harder, which makes it possible to compensate for the greater quantity of tissues to cross so that the neutrons arrive at the tumor with an energy favoring the captures on the ^{10}B . It is thus observed that the shape of the spectra at the exit of the moderator is coupled with the details of its structure. The TopOpt algorithm cleverly adjusts the energies and directions of the neutrons exiting the moderator to minimize exposure of healthy tissue.

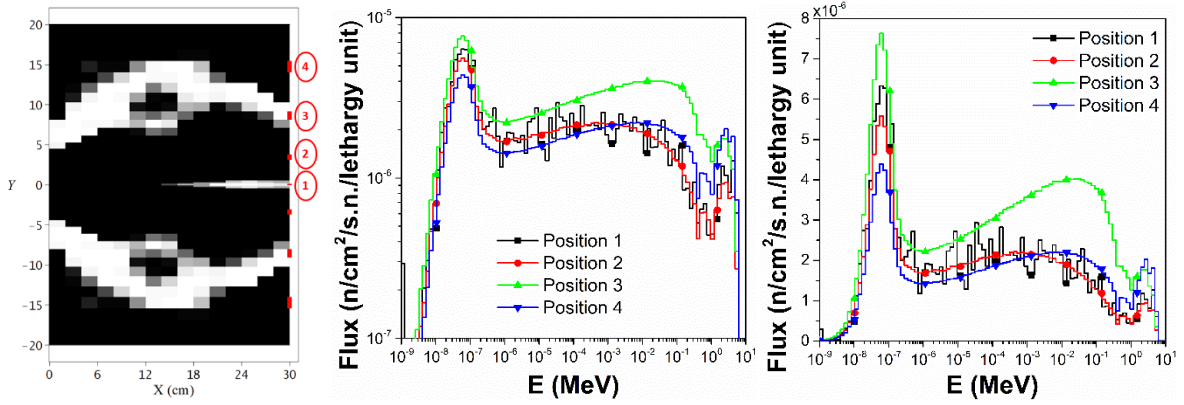


Figure 7. Energy spectra, in neutron(n)/cm²/s.n./lethargy unit, in log-log and log-lin scales, at the exit of the TopOpt moderator obtained for $N = 375$, $P_{tum} = 4.5$ cm and $H = 30$ cm, at positions 1 to 4 indicated on the left.

3.3. Exploration of several parameters

In this section, we will show how the shape of the moderator and the quality of treatment evolve with the maximum available thickness H or with the depth P_{tum} of the tumor. These studies will illustrate one of the strengths of the TopOpt approach, which allows it to fit the design of the moderator to the various possible configurations of a BNCT treatment unit, as well as to the various biological parameters of its patients, including the nature of the neutron source used, the volume and the depth of the tumors to be treated, the structures of patients' heads, or the time and possible fractionation of the treatment, among many other parameters.

3.3.1. Evolution of the structure and efficiency of a TopOpt D₂O moderator with its thickness

The calculations presented in section 3.2 were carried out for a thickness, $H = 30$ cm, of the moderator and concrete wall. This thickness has not been set arbitrarily: its order of magnitude comes from the work of Hervé et al. [8], who showed that a heavy water hemisphere of ~ 30 cm in radius moderates neutrons enough to deposit a high dose in the tumor while limiting the exposure of normal brain tissue. However, one can wonder how the shape and performances of an optimal D₂O moderator evolve with thickness H .

Fig. 8 (left), we present the TopOpt configurations obtained for $N = 375$ voxels and $P_{tum} = 4.5$ cm, by varying H between 20 and 40 cm. The corresponding maps of the total doses D_i (resp. dose excesses E_i) in each voxel of the head are presented in fig. 8 (center) (resp. right). We observe fig. 8 a foreseeable evolution of the optimal shape of the moderator with H . For low thicknesses, $H \leq 20$ cm, the too small available volume does not allow the algorithm to keep the central needle visible fig. 4, which is replaced in favor of a compact moderation body. Conversely, for high H values, there is more volume than necessary to slow down the neutrons. The algorithm has more room, and can create more complex and more efficient structures. In all cases, whatever the value of H , we observe that the algorithm systematically recreates a neutron tunnel similar to that shown fig. 4, which mimics a multi-field exposure.

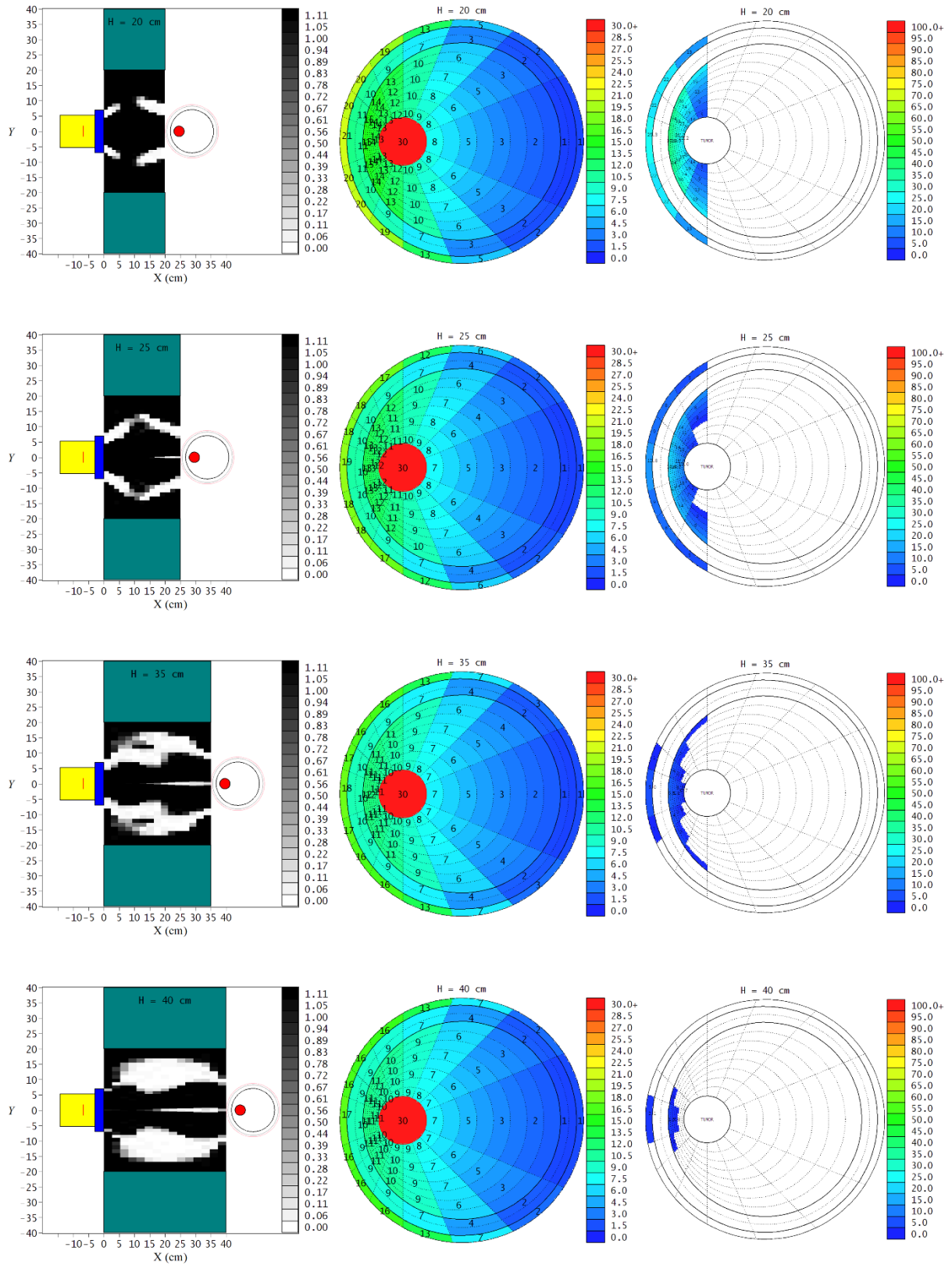


Figure 8. (Left) configurations of the TopOpt D₂O moderators obtained for $N = 375$ voxels, $P_{tum} = 4.5$ cm and $H = 20, 25, 35$ and 40 cm; (center) corresponding maps of the total doses, D_i , in Gy-Eq deposited in the patient's head; (right) corresponding maps of the dose excesses, E_i , in percent.

Fig. 9, we present the dose-volume histograms obtained in normal brain (left) and scalp (right) as a function of H , for $N = 375$ voxels and $P_{tum} = 4.5$ cm. We note the cleanliness of the treatments obtained for $H \geq 30$ cm. For $H = 40$ cm e.g., the doses exceed the most conservative peak doses, 11 Gy-Eq (brain), 30 Gy-Eq (skull), 16.7 Gy-Eq (scalp), only in 0.41% of the volume of the patient's head, and this by little, +1-2% max.

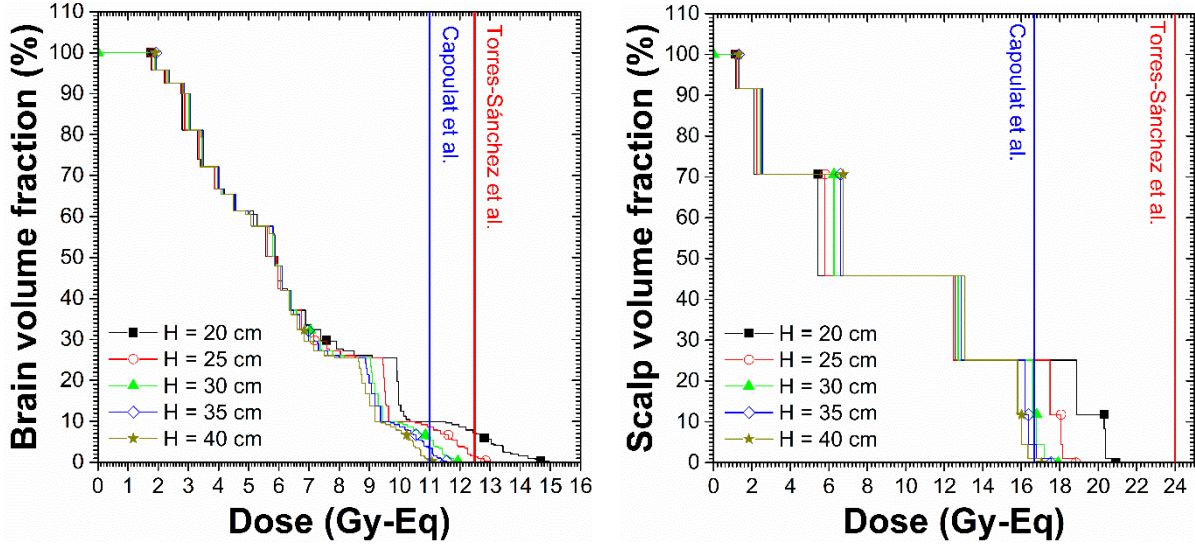


Figure 9. Dose-volume histograms in normal brain (left) and scalp (right), obtained for the TopOpt moderator calculated for $P_{tum} = 4.5$ cm, $N = 375$ voxels and $H = 20, 25, 30, 35, 40$ cm.

Fig. 10, following the methodology described in section 3.2.4, we plot the total doses delivered in healthy (left) and tumor (right) brain tissues as a function of the depth P along the beam axis, for $H = 30$ and 40 cm. As a reminder, in fig. 10, the origin $P = 0$ cm is the point (closest to the moderator) where the beam axis intersects with the surface of the brain, and is therefore located at a depth of 1.66 cm from the surface of the patient's head.

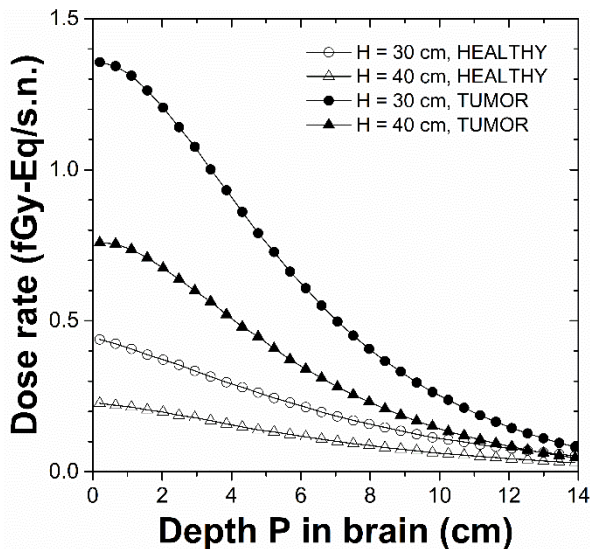


Figure 10. Total doses, in fGy-Eq/s.n., delivered in healthy and tumor brain tissues positioned at a depth P in brain along the beam axis, obtained for the TopOpt moderators calculated for $P_{tum} = 4.5$ cm, $N = 375$ voxels and $H = 30, 40$ cm. The origin, $P = 0$ cm, is on the brain surface, therefore 1.66 cm deep from the surface of the patient's head.

We also give Table 3 the evolution of F_{PEN} and D_{tum} with H . The corresponding treatment times T , necessary to reach 30 Gy-Eq in the tumor with 30 mA of beam intensity, are also indicated. As one would expect, the more the thickness of the moderator increases, the better the neutrons are moderated and guided, the cleaner the treatment. But at the same time, the more H increases, the lower the neutron flux at the exit of the moderator, the longer the treatment. The choice of the thickness of the moderator will therefore require a compromise between the therapeutic objective (minimization of exposure to healthy tissues) and the economic objective (minimization of treatment time).

H (cm)	F_{PEN}	D_{tum} (fGy-Eq/s.n.)	T (min)
20	6.10×10^1	2.19	23
25	1.57	1.43	35
30	1.89×10^{-1}	1.05	48
35	7.84×10^{-2}	0.797	63
40	2.99×10^{-2}	0.590	85

Table 3. Evolution with H of the penalization function F_{PEN} , the dose rate at tumor D_{tum} and the treatment time T , obtained with the TopOpt moderators generated fig. 8 for $P_{tum} = 4.5$ cm and $N = 375$ voxels.

3.3.2. Evolution of the structure and efficiency of a TopOpt D₂O moderator with tumor depth

In this section, we will study how the optimal shape of the D₂O moderator and the associated treatment cleanliness evolve with the depth P_{tum} of the tumor. For this study, which is costly in computing power, we reduced the number N of voxels of the moderator to 150. As the volume of moderator voxels is subsequently increased, the MCNP simulations can be run with a lower number of source neutrons, 2×10^9 . This reduction in the spatial resolution makes it possible to reduce the computation time per P_{tum} value to ~ 15 days, instead of 2 months beforehand. The considered P_{tum} depths vary from 3.5 cm (CTV in contact with the skull) to 8.5 cm (CTV at the center of head). The thickness H of the moderator is set at 30 cm. The TopOpt configurations obtained are presented in fig. 11.

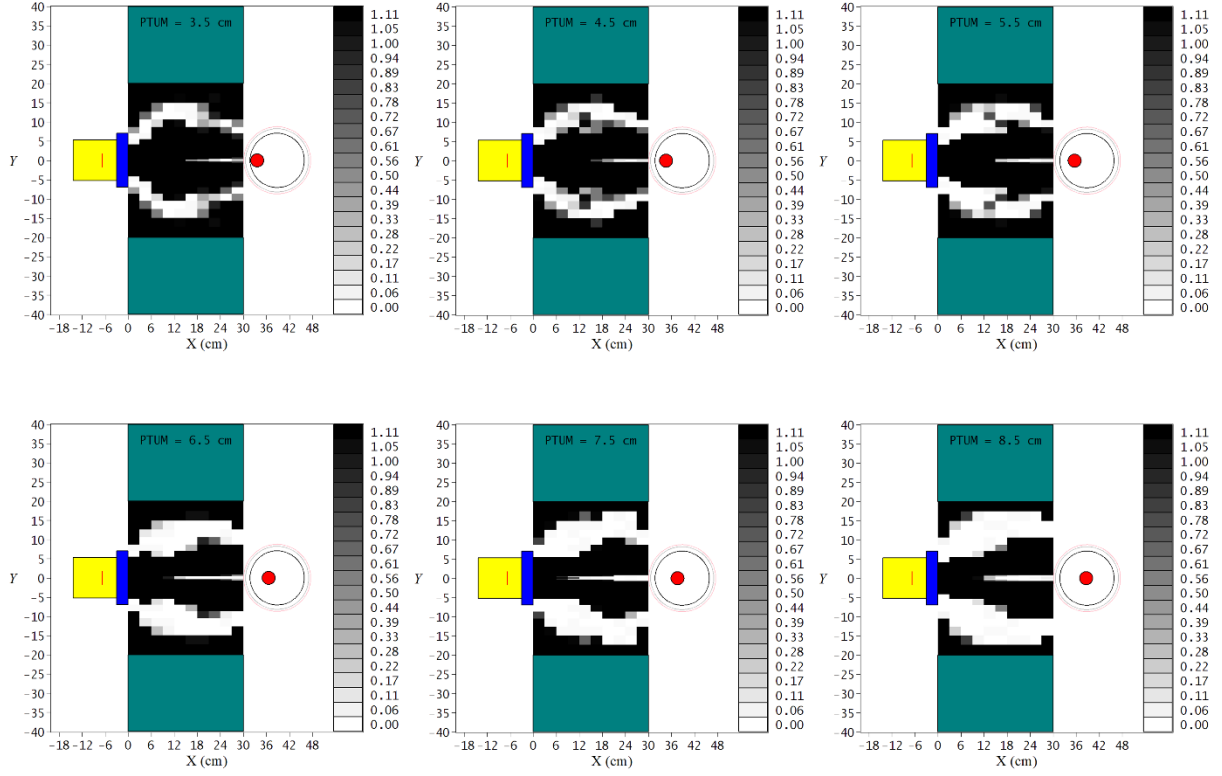


Figure 11. Configurations of the TopOpt D₂O moderators obtained for $N = 150$ voxels, $H = 30$ cm and P_{tum} ranging from 3.5 to 8.5 cm.

For $P_{tum} = 3.5$ to 8.5 cm, we observe fig. 11 that the algorithm recreates a moderation body, a reflector, a neutron tunnel and a central needle, as discussed in section 3.2. At 5.5 cm, however, a topology transition occurs; the moderator shape evolves to be closer to that of a moderated gun, whose moderation volume decreases as P_{tum} increases. Such a development is consistent with the fact that the deeper the tumor, the harder the neutron energy spectrum must be to reach it.

In fig. 12, we present the dose-volume histograms obtained for normal brain (left) and scalp (right) for each depth. For $P_{tum} \leq 5.5$ cm, the treatment maintains a good degree of cleanliness, with doses exceeding peak values only in a small volume of the patient's head, and by little. Beyond that, the quality of treatment deteriorates. For tumors deeper than 5.5 cm, it will probably be necessary to modify the thickness H and the radius (so far set at 20 cm) of the moderator, as suggested by the perhaps too small thickness of the reflectors visible in fig. 11. Materials other than heavy water will also have to be tested, which may perform better at very high depths. This specific study will be conducted as part of a project currently being submitted.

We give Table 4 the evolutions of the F_{PEN} penalization function and the D_{tum} dose rate with P_{tum} . The corresponding treatment times T , necessary to reach 30 Gy-Eq in the tumor with 30 mA of beam intensity [7], are indicated.

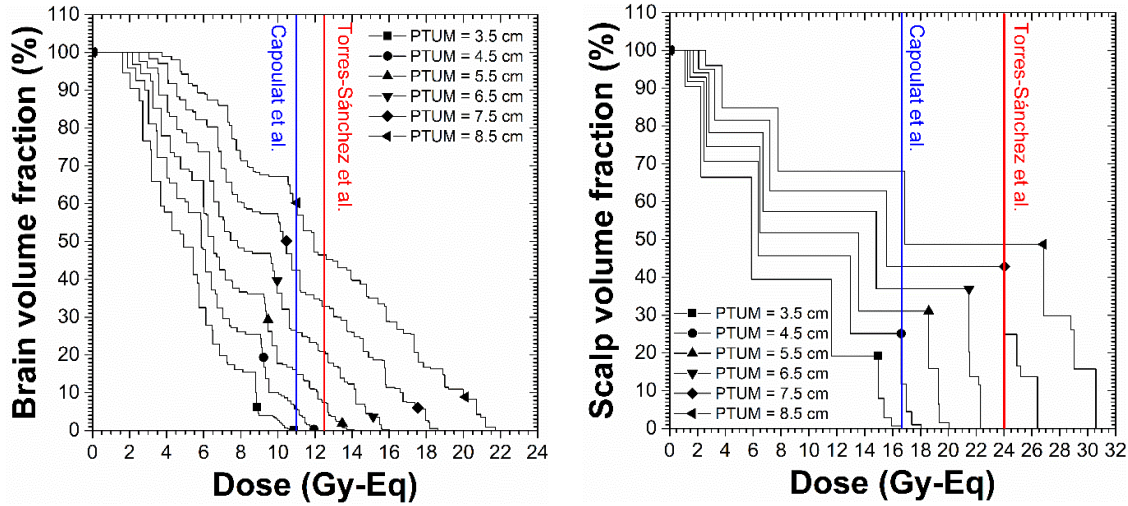


Figure 12. Dose-volume histograms in normal brain (left) and scalp (right), obtained for $N = 150$ voxels, $H = 30$ cm and P_{tum} ranging from 3.5 to 8.5 cm.

P_{tum} (cm)	F_{PEN}	D_{tum} (fGy-Eq/s.n.)	T (min)
3.5	6.10×10^{-3}	1.12	45
4.5	2.24×10^{-1}	1.05	48
5.5	1.38×10^1	0.997	51
6.5	1.08×10^3	0.846	60
7.5	1.41×10^5	0.742	68
8.5	1.66×10^7	0.675	75

Table 4. Evolution with P_{tum} of the penalization function F_{PEN} , the dose rate at tumor D_{tum} and the treatment time T , obtained with the TopOpt moderators generated fig. 11 for $H = 30$ cm and $N = 150$ voxels.

3.4. Manufacture of a TopOpt D2O moderator

The densities ρ_j of heavy water obtained by topology optimization in the moderator voxels vary between 0 and ρ_{max} , the density of heavy water. Strictly compliant manufacture of a TopOpt moderator will therefore require the use of porous materials, e.g. beads of varying sizes, or alveolar media manufactured by 3D printing. Such technologies exist, cf. e.g. [24, 25]. However, a simplification of the design, of the binary type, where we force each moderator voxel to contain either 0% or 100% heavy water, would, at least initially, be easier to machine.

Fig. 13 (left) shows such a simplification, for the design obtained for $H = 30$ cm and $P_{tum} = 4.5$ cm, by taking $\rho_j = \rho_{max}$ if $\rho_j > \rho_{max}/2$, $\rho_j = 0$ otherwise. The F_{PEN} value obtained for this simplified configuration, called TopOpt Black & White (BW), is equal to 0.1998 ± 0.0062 , vs. 0.1892 ± 0.0058 for the original TopOpt configuration. These two values are statistically compatible, the simplification of the design does not lead to a significant deterioration in the quality of treatment. This result is consistent, since apart from a few border voxels, the TopOpt design shown in fig. 4 is already predominantly binary.

This simplification of the design facilitates the manufacturing of the TopOpt moderator. One possible solution is to machine, e.g. from aluminum or steel, a cylindrical tank 20 cm in radius and 30 cm in length. The neutron tunnel and the central needle of the TopOpt BW moderator can then be 3D printed and positioned in the tank, which is then filled with heavy water (32 liters for the design in fig. 13). We give fig. 13 (right) a photo of a section of the neutron tunnel,

printed in PLA using a RAISE3D machine from the CNRS LPSC printing platform. There is a small hole, made for the heavy water to fill the ring in the neutron tunnel visible in fig. 4 or 13.

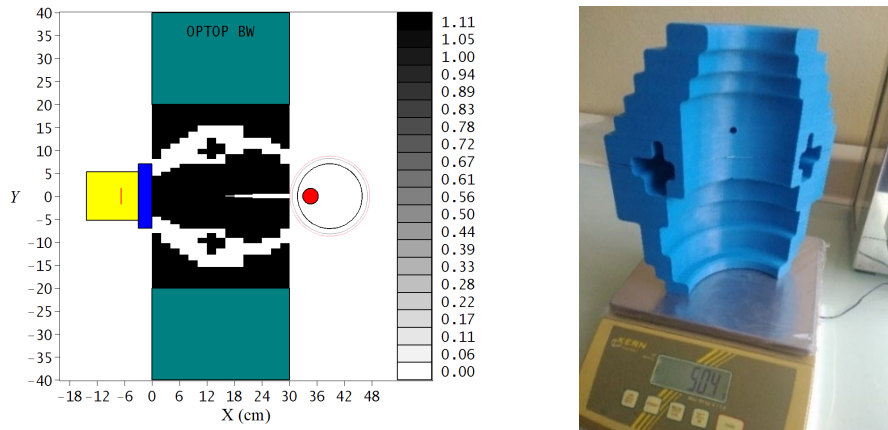


Figure 13. (Left) BW design of the TopOpt moderator calculated for $N = 375$ voxels, $P_{num} = 4.5$ cm and $H = 30$ cm; (right) 3D printing in PLA of a section of the neutron tunnel of this moderator.

5. Conclusion and perspectives

In this study, we applied a topology optimization algorithm developed at the CNRS LPSC to compute the structure of a heavy water neutron moderator for an AB-BNCT unit, for various tumor depths or moderator thicknesses.

Calculations performed for deep glioblastomas using a ${}^9\text{Be}(d(1.45 \text{ MeV}), n){}^{10}\text{B}$ source give convincing results. Despite the high energy, ~ 2 MeV in average and up to 6 MeV, of the source neutrons, the TopOpt moderators manage, in a compact volume, less than 0.04 m^3 , to deliver targeted doses, which reach 30 Gy-Eq in the tumor in a reasonable time while sparing healthy tissues. The local doses deposited in these tissues remain below the recommended limits, in almost the entire head volume, for tumor depths of up to 6 cm at this time.

TopOpt moderators have sophisticated structures, inaccessible in their detail to intuition or to previous parametric methods. They contain unexpected components, e.g. neutron tunnels mimicking multi-field treatments, the efficiency of which could inspire other designs. The progress made in manufacturing processes, 3D printing for example, now makes the machining of such components accessible to a small structure, laboratory or hospital unit. The versatility of the TopOpt approach makes it possible to automatically fit the design of the moderator to the configuration of the BNCT treatment unit considered (e.g. the neutron source and materials it uses) as well as to the biological parameters of the patients (e.g. the volume and depth of the tumor to be treated, or the characteristics of the targeted organs).

However, despite these first promising results, progress remains to be made, on the computation time, on the head model, or on the maximum tumor depth that can be properly reached. As such, we plan to study, as part of a submitted project, materials other than heavy water that could be of therapeutic and economic interest. Heavy water is indeed an efficient material for slowing down neutrons in a compact volume without capturing them, but it remains expensive and is a special nuclear material.

Acknowledgments

We would like to thank Véronique Ghetta, CNRS LPSC, for her advice and the driving role she played in initiating this work.

Bibliography

- [1] IAEA-TECDOC-1223, *Current status of neutron capture therapy*, 2001
- [2] W.A.G. Sauerwein et al. (editors), *Neutron capture therapy: principles and applications*, Springer Science & Business Media, 2012
- [3] R.F. Barth et al., *Radiat. Oncol.* 7 (2012) 146
- [4] T.D. Malouff et al., *Front. Oncol.* 11 (2021) 601820
- [5] J.A. Coderre et al., *Applied Radiation and Isotopes* 61 (2004) 1083–1087
- [6] P. Torres-Sánchez et al., *Scientific Reports* 11 (2021) 7576
- [7] M.E. Capoulat et al., *The $^9\text{Be}(d,n)^{10}\text{B}$ reaction as a neutron source for Boron Neutron Capture Therapy*, 10th Latin American Symposium on Nuclear Physics and Applications, 2014, available at: <https://pos.sissa.it/194/025/pdf> (last accessed: January 2022)
- [8] M. Hervé, *Fast and epithermal neutron fields for Accelerator Based Neutron Capture Therapies*, PhD thesis, Université Grenoble Alpes, 2021, available at <https://tel.archives-ouvertes.fr/tel-03426753> (last access: January 2022)
- [9] M.E. Capoulat et al., *Nuclear Instruments and Methods B* 445 (2019) 57-62
- [10] T. Goorley et al., *Nuclear Technology* 180 (2012) 298-315
General information about MCNP6, including the Users Manual of version 6.2, can be found at https://mcnp.lanl.gov/mcnp_manual.shtml (last access: January 2022)
- [11] Y. Sakurai et al., *Nucl. Instr. Meth. A* 453 (2000) 569-596
- [12] K.M.D. Bushby et al., *Centiles for adult head circumference*, *Archives of Disease in Childhood* 67 (1992) pp 1286-1287
- [13] M.S. Cohen, available at https://en.wikipedia.org/wiki/Human_head (last access: January 2022)
- [14] J.T. Goorley et al., *Med. Phys.* 29 (2002) 145
- [15] M.B. Chadwick et al., *Med. Phys.* 26 (1999) 974
- [16] ICRU Report 63, *Nuclear data for neutron and proton radiotherapy and for radiation protection*, 2000
- [17] F.H. Attix, *Introduction to radiobiological physics and radiation dosimetry*, Wiley-VCH, 1986, in Chapter 4, pp 61-79
- [18] NISTIR Report 5632, *Tables of X-Ray mass attenuation coefficients and mass energy-absorption coefficients 1keV to 20 MeV for elements Z=1 to 92 and 48 additional substances of dosimetric interest*, 1995
- [19] G.D. Kerr, *Photon and neutron fluence-to-kerma conversion factors for ICRP-1975 reference man using improved elemental compositions for bone and marrow of the skeleton*, Report ORNL/TM-8318, ORNL, 1982
- [20] From P. Rubin, in W. Small et al., *Radiation toxicity: a practical medical guide*, Springer US, 2006, pp 24
- [21] P.R. Menéndez et al., *Applied Radiation and Isotopes* 67 (2009) S50–S53
- [22] S. Chabod, *Nucl. Instr. Meth. A* 931 (2019) 181-206
- [23] S. Chabod, *J. Nucl. Eng.* 2 (2021) 152-160
- [24] J. Madamesila et al., *Physica Medica* 32 (2016) 242–247
- [25] IceSL slicer, in *Progressive infils*, available at <https://icesl.loria.fr/features/> (last access: January 2022)

Appendix

In this Appendix, we present a set of sensitivity studies, useful for evaluating the robustness of the TopOpt calculations. We have explored the sensitivity of the quality of treatment to the details of the structure of a TopOpt moderator, to the voxelization of the patient's head, to the parameterization of the F_{PEN} function, to the uncertainties on transport data and to the morphological diversity of the patients.

A.1. Robustness of the topological optimization

A.1.1. Global or local optima?

The moderator shapes computed in section 3 are complex but proved efficient. One can nevertheless legitimately wonder if each of these shapes really constitutes a global optimum of the optimization problem (2), and not a local optimum. Could there be even more efficient shapes? The TopOpt algorithm is a complex iterative algorithm, and predicting the outcome of an iterative algorithm, even a very simple one, is in the vast majority of cases impossible, cf. Langton's ant or Syracuse conjecture. Nonetheless, there are arguments in favor of the global optimum. In Ref. [22], we verified, for several optimization problems constructed to have a solution obvious to a human or an analytical solution that the TopOpt algorithm does indeed reach the global optimum. In addition, it is possible to test the robustness of the solutions found, e.g. the solution proposed in fig. 4, by modifying some geometry details, for example by removing the D₂O ring or the central needle described in section 3.2, then by looking at the impact of these modifications on the treatment quality. The geometries of these modified moderators are presented in fig. A.1. The F_{PEN} values obtained are 0.2030 ± 0.0063 (no needle) and 0.2202 ± 0.0067 (no ring), against 0.1892 ± 0.0058 for the TopOpt moderator. We see a degradation in the cleanliness of the treatment, indicating that the intricacies of the structure of a TopOpt moderator (at least this one) are not superfluous.

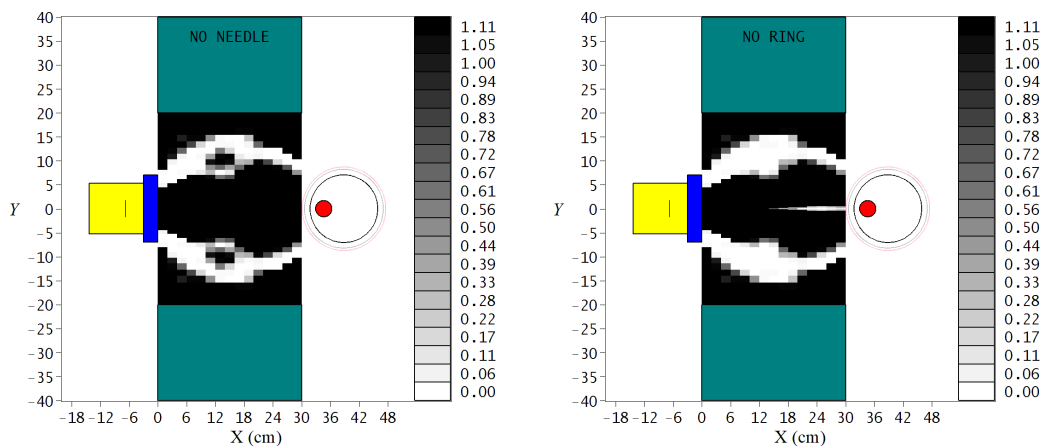


Figure A.1. (Left) design obtained by removing the central needle in the TopOpt moderator shown fig. 4; (right) design obtained by removing the D₂O ring in the neutron tunnel of the TopOpt moderator shown fig. 4.

A.1.2. Existence of dose hot spots?

The head model used in this study, presented in section 2 and fig. 1, is composed of $M = 89$ voxels: 1 for the tumor, 88 for the normal tissues. Even if its axial symmetry eliminates the need for a discretization in angles around the axis, one can legitimately wonder if this small

number of voxels can mask, by averaging it on the volume of a voxel, a (or several) local deposit of very high dose, of the hot spot type, in particular in tissues located near the exits of the moderators. To study this possibility, we took the TopOpt moderator shown fig. 4, and recalculated with it the doses deposited in a head model comprising $M = 881$ voxels, 1 for the tumor, 880 for the normal tissues, drawn in fig. A.2 (left). The resulting map of dose excesses is given fig. A.2 (left). By comparing it with that obtained in fig. 3 for $M = 89$, we see no hot spot, only a slight increase in the dose delivered in the scalp in front of the central needle, cf. fig. 4. To complete the analysis, we plot fig. A.2 (right) the dose-volume histograms in normal brain and scalp obtained for $M = 89$ and 881. We again note a slightly higher dose deposition in an area encompassing 0.04% of the volume of the scalp, located in front of the central needle. We therefore retained $M = 89$ in this study, a value which ensures a compromise between the spatial resolution of the dose deposition and the large computation time (as a reminder, 2 months for a TopOpt computation with $N = 375$ and $M = 89$, against ~ 20 months probably if a TopOpt computation was performed with $N = 375$ and $M = 881$).

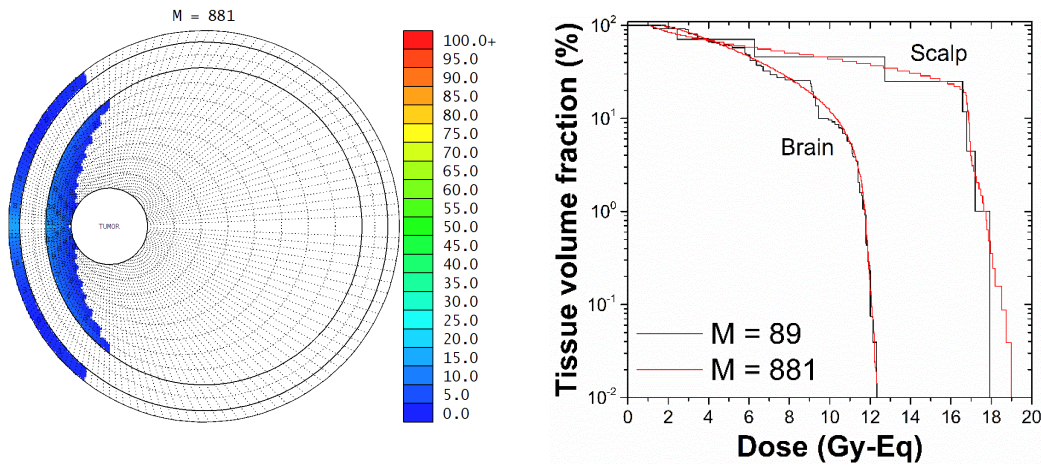


Figure A.2. (Left) map of the dose excesses E_i , in %, obtained for the head model with $M = 881$ voxels and the TopOpt moderator shown fig. 4; (right) dose-volume histograms in normal brain and scalp, obtained for $M = 89$ and 881 voxels.

A.1.3. Sensitivity to optimization parameters?

The TopOpt moderators presented in section 3 were obtained by minimizing the F_{PEN} function formulated in Eq. (2). This formulation of F_{PEN} is a human choice, reasoned, but which constitutes nonetheless a weak point. One can legitimately wonder if the shapes and performance of moderators could be significantly improved with a different formulation of F_{PEN} . Here again the question of the global character of the calculated optima arises. Ideally, to answer this question, it would be necessary to propose a large number (~ 100) of different yet credible F_{PEN} formulas, to compute for each of them the shape and the properties of the TopOpt moderator, then to conclude on the robustness of the design to the choice of the formulation of the optimization problem. Such a study would however require a gigantic computing power, which would amount in decades per 24 CPUs server. For the time being, we therefore propose a less ambitious but more economical study, which consists in keeping the formulation (2) of F_{PEN} , but by modifying the only parameter which is arbitrarily chosen there, the number n . Indeed, the only condition on n is that it is $\gg 1$. To do this, we recalculated the shape of the optimal moderator for $H = 30$ cm, $N = 150$ voxels, $P_{tum} = 4.5$ cm, this time taking $n = 200$ instead of 30 so far. The configuration of the TopOpt moderator thus obtained is shown fig. A.3

(left); the corresponding maps of doses and dose excesses in the head voxels are presented in fig. A.3 (center and right).

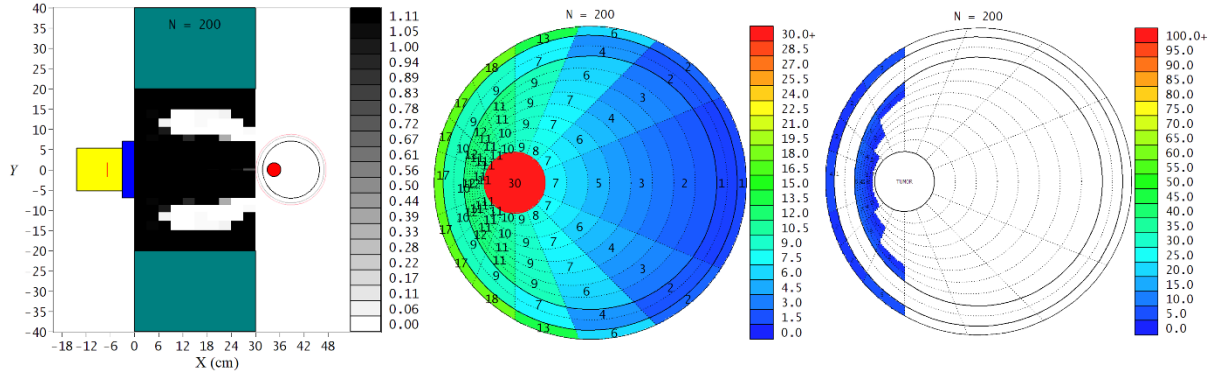


Figure A.3. (Left) configuration of the TopOpt D₂O moderator obtained for $N = 150$ voxels, $H = 30$ cm, $P_{tum} = 4.5$ cm and $n = 200$; (center) corresponding map of the total doses, D_i , in Gy-Eq deposited in the patient's head; (right) corresponding map of the dose excesses, E_i , in percent.

Compared to the design shown fig. 11 for $n = 30$, we note an evolution in the shape of the moderator, with a reduction in the length of the neutron tunnel and the central needle, both in favor of a larger moderation volume. However, these design changes do not lead to a significant change in the quality of treatment, as can be seen by comparing the maps of the dose excesses fig. 11 for $n = 30$ and fig. A.3 for $n = 200$. By recalculating F_{PEN} with $n = 30$ for the design shown fig. A.3, we get $F_{PEN} = 0.2367 \pm 0.0124$, against 0.2245 ± 0.0112 for the design shown fig. 11, two values compatible in their error bars. The treatment quality therefore seems not very sensitive to the choice of the number n , which constitutes a first element of response on the robustness of the optimization to the formulation of F_{PEN} . However, we observe that the D_{tum} dose rate obtained for the design shown fig. A.3 is equal to 0.9468 ± 0.0016 fGy-Eq/s.n., against 1.0495 ± 0.0017 fGy-Eq/s.n. for the design shown fig. 11. The treatment time for the TopOpt design with $n = 200$ is therefore increased by 10% compared to the TopOpt design with $n = 30$. Taking a value of n that is too large is therefore counterproductive. Indeed, for very large n values, function F_{PEN} varies considerably during convergence, over 70 orders of magnitude for $n = 200$: $F_{PEN} = (2.6 \pm 1.4) \times 10^{74}$ at NUMITER = 0, $(9.7 \pm 3.9) \times 10^{51}$ at NUMITER = 10, $(4.0 \pm 1.8) \times 10^3$ at convergence. Above all, its values are affected by very large statistical errors, since they grow proportionally with n (derivative of F_{PEN}). Such variations and stat. uncertainties alter the convergence of the algorithm, by penalizing in a counterproductive way the transfers of matter between the voxels of the moderator which would make it possible to exceed, even slightly, the peak doses at a place of the patient's head, to significantly reduce exposure elsewhere. We therefore kept $n = 30$ throughout the study, a reasonable value which satisfies the condition $n \gg 1$ while limiting the statistical error on F_{PEN} at a few %.

A.2. Sensitivity to nuclear data

We will address here the question of the uncertainty on the calculated quality of treatment induced by the uncertainties on the transport data. These transport data are produced through models whose use or parameters can differ from one evaluator to another. They are affected by statistical and systematic uncertainties, due to imperfections or unknowns in the experimental devices used to measure them, to statistical fluctuations in measurements, to approximations in modeling and analysis, etc. Carrying out such a sensitivity analysis & uncertainty quantification

study is a considerable work, which goes beyond the scope of this study. To address this nonetheless important question, we propose here a simplified and common approach, which consists in performing the calculations using several different databases, then in comparing the results obtained.

For this study, we used the moderator shown fig. 4, obtained for $N = 375$ voxels and $P_{tum} = 4.5$ cm, using transport data from the ENDF/B-VII.0 database (/B-VI.6 for ^1H and ^{138}Ba), cf. section 2. We then recalculated the doses deposited in the patient's head, the F_{PEN} function, and the D_{tum} dose rate in fGy-Eq/s.n., using two other databases, JEFF-3.1 and JENDL-3.3. This study required some adjustments: (i) as JENDL-3.3 lacks the gamma-ray production cross-sections for ^2H , ^{35}Cl , ^{37}Cl and ^{138}Ba (.42c), we used for these isotopes data from ENDF/B-VII.0 & /B-VI.6 (.70c for ^2H , ^{35}Cl , ^{37}Cl , .66c for ^{138}Ba); (ii) same for ^{138}Ba in JEFF-3.1 (.03c), replaced by ENDF/B-VI.6 (.66c); (iii) The $S(\alpha,\beta)$ thermal data were all taken from ENDF (hwtr.10t for the moderator, grph.10t and al27.12t for the source casing, lwtr.10t for the head).

Fig. A.4, we give, as a function of the voxel number i , the relative deviations, $D_i(x)/D_i(\text{ENDF}) - 1$, with $x = \text{JENDL-3.3}$ or JEFF-3.1 , between the ^{10}B , $^{14}\text{N}(n,p)$, neutron (without $^{14}\text{N}(n,p)$), γ and total doses, calculated with ENDF/B-VII.0 & /B-VI.6, JEFF-3.1 and JENDL-3.3 (note: these are doses expressed in Gy-Eq, obtained by setting the total dose $D_{i=0}$ deposited in the tumor at 30 Gy-Eq, see fig. A.4). We observe that, whatever the voxel $i > 0$ considered, the JEFF-3.1 and JENDL-3.3 total doses are systematically lower than the ENDF total doses, sometimes significantly (note: with the exception of voxels 80 and 88 for JEFF-3.1, where the deviations appear positive but are in fact consistent with 0 in the statistical error bars). It follows that the treatments predicted with JEFF-3.1 and JENDL-3.3 are cleaner than that predicted with ENDF, but also a little longer, as shown by the values of F_{PEN} and D_{tum} calculated for these 3 databases given table A.1. It is probable that JENDL-3.3 underestimates the exposure of healthy tissues, because its data, particularly of gamma-ray production, are less complete. The difference between JENDL-3.3 and ENDF gamma doses is clearly visible in fig. A.4 (left). Throughout our study, we adopted a conservative approach, consistently using the most unfavorable database, ENDF/B-VI.6 & VII.0, as it predicts a higher exposure to healthy tissues than JENDL-3.3 or JEFF-3.1.

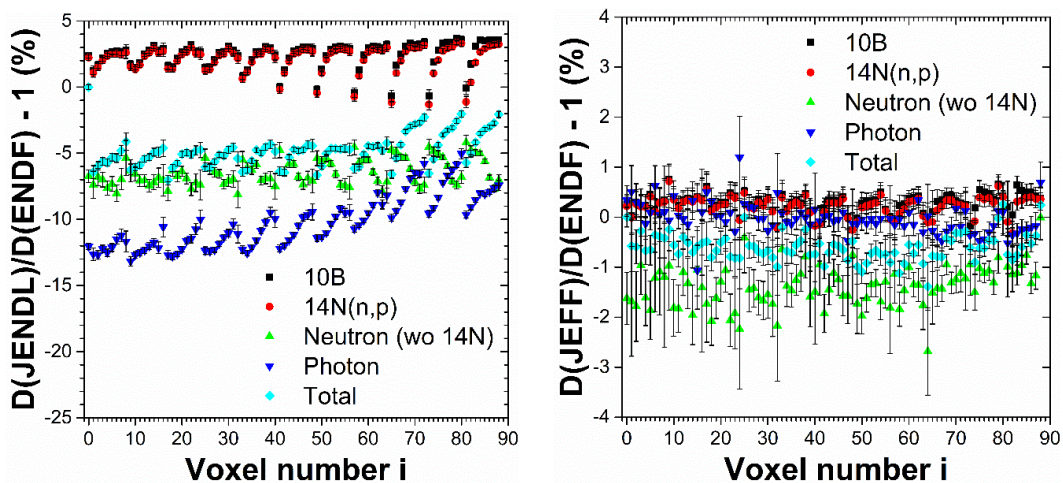


Figure A.4. Deviations in % between the ^{10}B , $^{14}\text{N}(n,p)$, neutron (w/o $^{14}\text{N}(n,p)$), γ and total doses, calculated for the TopOpt moderator of fig. 4 with the ENDF/B-VI.6 & VII.0 and JENDL-3.3 databases (left), and with the ENDF/B-VI.6 & VII.0 and JEFF-3.1 databases (right). Note: the tumor voxel is the voxel $i = 0$, brain is $i = 1 \dots 64$, skull is $i = 65 \dots 80$, scalp is $i = 81 \dots 88$.

Database	F_{PEN}	D_{tum} (fGy-Eq/n.s.)
JENDL-3.3	0.0573 ± 0.0018	1.0089 ± 0.0010
JEFF-3.1	0.1595 ± 0.0049	1.0412 ± 0.0010
ENDF/B-VI.6&VII.0	0.1892 ± 0.0058	1.0499 ± 0.0010

Table A.1. Values of F_{PEN} and D_{tum} obtained for the TopOpt moderator shown fig. 4 ($N = 375$ voxels, $P_{tum} = 4.5$ cm), computed with the JENDL-3.3, JEFF-3.1 or ENDF/B-VI.6&VII.0 databases.

A.3. Sensitivity to morphological parameters

The TopOpt moderators obtained in the previous sections were computed using a simplified model of the patient's head, presented and discussed section 2. The shape and composition of a real human head are much more complex, so one can legitimately wonder what impact this simplification, common to any analytical or even voxelized model, can have on the quality of treatment. In addition, the morphology of a human head varies considerably from patient to patient. It is therefore interesting to study how (1) the modeling of the head and (2) the great morphological variability of patients can impact the design of the moderator and its associated treatment quality. The TopOpt procedure presented in this study may provide an element of solution to these problems, thanks to its adaptability. In this section, for the time being, we propose to provide an element of response to the problem (2).

To answer this, we generated 92 different patients' heads, by independently sampling for each patient its brain radius R_b , its skull radius R_s and its head radius R_h , according to Gaussians of centers $\langle R_b \rangle = 7.05$ cm, $\langle R_s \rangle = 8.21$ cm and $\langle R_h \rangle = 8.71$ cm, and 5.35% standard deviation. These values comply with Ref. [12, 13], which give size distributions of adult heads. However, since a variable distributed according to a Gaussian can take any value between $-\infty$ and $+\infty$, we have prohibited values of R_h less than $0.899 \times \langle R_h \rangle$ (1st percentile) and greater than $1.115 \times \langle R_h \rangle$ (99th percentile) [13]. In the absence of data found on the minimum and maximum thicknesses of skull and scalp, R_b and R_s radii are sampled freely, provided that $R_b < R_s < R_h$. These 92 generated head configurations all have different radii, and different brain, skull or scalp volumes. For each of them, we have adapted the voxelization shown in fig. 1: 1 voxel for the CTV ($i = 0$), 64 for normal brain tissue ($i = 1 \dots 64$), 16 for the skull ($i = 65 \dots 80$), 8 for the scalp ($i = 81 \dots 88$), 89 in total. Each patient is positioned at the exit of the TopOpt BW moderator shown fig. 13. The positions of the centers of the heads are adjusted so that the minimum distance between the surface of the head and the exit of the moderator remains equal to 1 mm, cf. section 2. The volume of the CTV is equal to 20 cm^3 , its depth P_{tum} equal to 4.5 cm.

Fig. A.5, we plot the distributions of the dose-volume histograms obtained in normal brain and scalp for the 92 patients, indicating the 1st, 5th, 25th, 50th, 75th, 95th and 99th percentiles. We find that the doses deposited in the brain exceed the peak dose used by Capoulat et al. [7], 11 Gy-Eq, only in a small fraction of the brain for all patients. Doses exceed the peak dose used by Torres-Sánchez et al. [6], 12.5 Gy-Eq, in 25 out of 92 patients. However, for 23 of these 25 patients, the affected brain volume is negligible, less (or even much less) than 0.2%. For 2 out of 92 patients, who thus stand out exceptionally, the volume of brain exposed to a dose higher than 12.5 Gy-Eq reaches 4.7% for one, 4% for the other. These 2 patients have unusual morphological parameters: (i) for the first, a small head, $R_h = 7.99$ cm (the 2nd smallest in the sample), and thin thicknesses of skull and scalp, resp. 4.1 mm and 0.5 mm; (ii) for the second, an abnormal skull thickness, 1.3 mm, and radiuses of brain, skull and head, 7.60 cm, 7.73 cm and 8.30 cm, all quite far from the average values. The findings are similar for scalp. The doses deposited in the scalp never exceed the peak dose used by Torres-Sánchez et al. [6], 24 Gy-Eq.

They remain below 18 Gy-Eq in the bulk of the scalp volume for all patients. These results are important and rarely presented in the literature. They show that, for a tumor of intermediate depth, here 4.5 cm, reusing a moderator designed for a generic model patient, whose head has the standard proportions, will most often have no major harmful impact on the healthy tissues of a random patient, whatever its morphology of his head. However, for a fraction of patients, of the order of a few percent, side effects are to be feared, either in the brain or in the scalp.

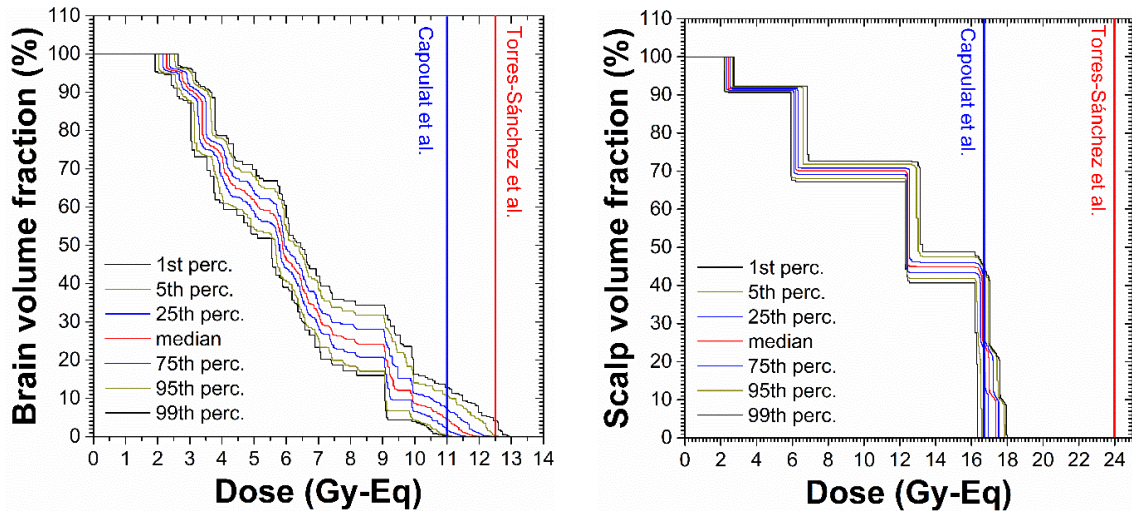


Figure A.5. Distributions of the dose-volume histograms in normal brain (left) and scalp (right) obtained for the 92 patients, using the TopOpt BW moderator shown fig. 13 for $P_{tum} = 4.5$ cm and $H = 30$ cm.